UNIVERSITY *of* York

This is a repository copy of *Efficient Silicon Metasurfaces for Visible Light*.

White Rose
university consortium
Universities of Leeds, Sheffield & York

eprints@whiterose.ac.uk
https://eprints.whiterose.ac.uk/

Efficient Silicon Metasurfaces for Visible Light

Zhenpeng Zhou,[†,‡,||][ID] Juntao Li,[†,‡,||] Rongbin Su,[†,‡] Beimeng Yao,[†,‡] Hanlin Fang,[†,‡] Kezheng Li,[†,‡] Lidan Zhou,[†] Jin Liu,[†,‡] Daan Stellinga,[§] Christopher P. Reardon,[§] Thomas F. Krauss,[†,§] and Xuehua Wang*,[†,‡]

[†]State Key Laboratory of Optoelectronic Materials and Technologies and [‡]School of Physics, Sun Yat-Sen University, Guangzhou, 510275, China

[§]Department of Physics, University of York, York, YO10 5DD, U.K.

S *Supporting Information*
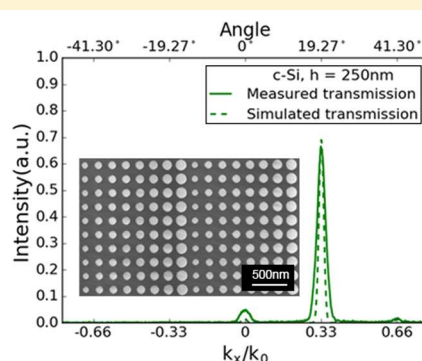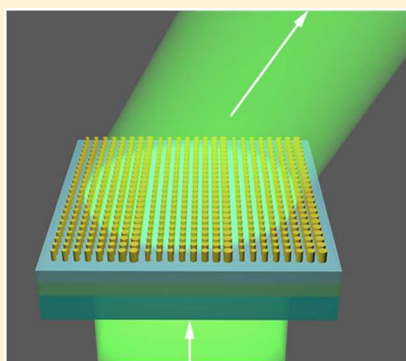
ABSTRACT: Dielectric metasurfaces require high refractive index contrast materials for optimum performance. This requirement imposes a severe restraint; either devices have been demonstrated at wavelengths of 700 nm and above using high-index semiconductors such as silicon, or they use lower index dielectric materials such as TiO_2 or Si_3N_4 and operate in the visible wavelength regime. Here, we show that the high refractive index of silicon can be exploited at wavelengths as short as 532 nm by demonstrating a crystalline silicon metasurface with a transmission efficiency of 71% at this wavelength and a diffraction efficiency of 95% into the desired diffraction order. The metasurfaces consist of a graded array of silicon posts arranged in a square lattice on a quartz substrate. We show full 2π phase control, and we experimentally demonstrate polarization-independent beam deflection at 532 nm wavelength. Our results open a new way for realizing efficient metasurfaces based on silicon for the technologically all-important display applications.

KEYWORDS: *dielectric metasurfaces, crystalline silicon, wavefront control, diffractive optics*

Metasurfaces are ultrathin optical elements that can manipulate optical wavefronts by modifying the phase, amplitude, or polarization of light waves on a subwavelength scale.[1−6] Metasurfaces offer new degrees of freedom for controlling light beams on a smaller scale and with higher accuracy than is possible with conventional bulky optical components. Initial demonstrations of metasurfaces involved plasmonic resonances, which, however, are rather lossy and exhibit low efficiency.[7,8] More recently, all-dielectric metasurfaces have come to the fore because of their high transmission.[9−11] Compared to plasmonic metasurfaces, they offer lower loss, yet they still exhibit Mie resonances for both polarizations at optical frequencies, which has been used to realize perfect reflectors,[12] magnetic mirrors,[13] and Huygens surfaces.[14,15]

Because of its high refractive index and compatibility with CMOS processes, silicon is widely used in all-dielectric metasurface devices, such as flat lenses,[16−18] achromatic lenses,[19] vortex generators,[20,21] holograms,[22−25] nonlinear devices,[26] and metasurfaces controlled phase and polarization independently.[27,28] However, most of the silicon metasurface work is performed in the near-infrared wavelength regime and not in the visible. This is because most researchers use amorphous silicon (a-silicon) or polycrystalline silicon (poly-silicon) due to the ease of deposition onto transparent substrates such as glass. The problem with deposited silicon is its high absorption loss in the visible regime. Thin-film crystalline silicon (c-silicon) offers a solution to this problem because of its much lower absorption at $\lambda > 500$ nm.[29,30] For example, the single-pass absorption of a 200 nm thin film of c-silicon and a-silicon is around 15% and 51% at a wavelength of 500 nm, respectively. The corresponding refractive index and extinction coefficient of c-silicon and a-silicon are $n_{c\text{-}si} = 4.295$, $k_{c\text{-}si} = 0.0719$[29] and $n_{a\text{-}si} = 4.497$, $k_{a\text{-}si} = 0.45526$.[11] While most researchers are aware that the absorption of c-silicon is lower

than that of a-silicon, it is not at all obvious that this difference is sufficient to enable the successful demonstration of high-efficiency metasurfaces in the visible regime. Meatsurfaces must create large phase delay in order to operate efficiently, and the large phase delays are typically achieved with large aspect ratio nanostructures. In the case of high refractive index absorbing materials such as silicon, the question arises whether a sufficient phase delay can be achieved in a given thickness of material without excessive absorption. Since the phase delay and absorption are a function of the entire nanostructure and not the thin film alone, this question can be answered only by considering the structure as a whole. Alternatively, titanium dioxide (TiO_2),[31−33] silicon nitride (Si_3N_4),[34] and silica (SiO_2)[35] have been used for all-dielectric metasurfaces based on their high transparency throughout the visible spectrum. For example, a 600 nm thin TiO_2 film has recently been patterned into nanofins and posts in order to form a high numerical aperture (NA) metalens for operation at visible wavelengths.[32,33] Due to the lower refractive index contrast compared to silicon, however, these TiO_2 nanofins and posts require very high aspect ratios of 10−15[32] and 6,[33] respectively, which makes the fabrication very challenging.

Here, we propose the use of thin-film c-silicon as a metasurface material for visible light operation and demonstrate high efficiency polarization-independent operation in transmission at 532 nm wavelength. This demonstration is enabled by our layer-transfer technique, whereby we transfer 220 and 250 nm c-silicon device layers from a silicon on insulator (SOI) wafer to a transparent quartz substrate. The maximum aspect ratio of our metasurfaces is 3.4 in the experiment, which makes it easier to fabricate than comparable devices based on Si_3N_4 or TiO_2. We believe that this method will open a new way to extend the functionalities of metasurfaces efficiently into the visible light regime.

To illustrate the capability of our c-silicon metasurface in transmission and its full 2π phase control, we consider light propagating through an array of circular c-silicon posts on a subwavelength square lattice (Figure 1).[16,27] Each post acts as Fabry−Pérot resonator, and different diameter posts support modes of different effective index. Due to the circular symmetry of the circular posts, our metasurfaces are polarization-independent.

We performed the numerical calculation using the rigorous coupled-wave analysis (RCWA) method[36] and analyzed the transmission coefficient and phase of the periodic c-silicon posts by varying the unit cell size a from 160 to 250 nm and the diameter from $0.2a$ to $0.8a$ at the wavelength 532 nm (Figure 2a,b). In the calculation, the post height h is fixed to be 220 nm (refractive index from ref 29), the thickness of the silica film (refractive index n_{Silica} = 1.45) and the adhesive NOA61 (Norland Products, Inc.) (n_{NOA} = 1.56) underneath are 1 μm, and the refractive index of the quartz substrate is 1.45. As shown in Figure 2, arrays of posts with 190 nm unit cell size can achieve large transmission amplitudes while spanning the full range of phases from 0 to 2π by varying the diameter of the posts from 38 to 152 nm. In Table 1, which is based on Figure 2c, we choose eight different diameter posts with $\pi/4$ increments to cover the full 0 to 2π phase range.

To validate the phase control effect of our c-silicon metasurfaces, we designed a prism-like refractive index gradient as a beam deflector using the eight phase elements shown in Table 1. The diffraction angle θ_t of such a gradient surface can be calculated via the generalized Snell's law,[8]

(a)

(b)
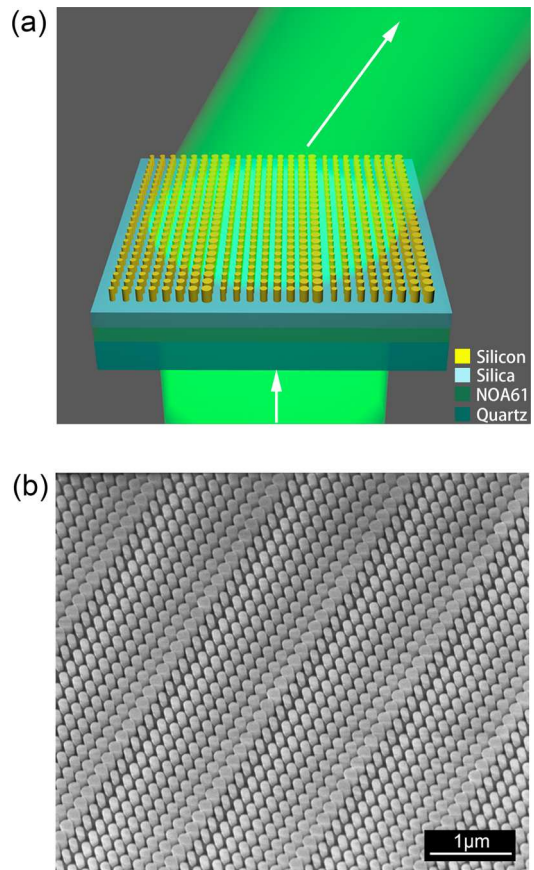
Figure 1. (a) Schematic of a gradient metasurface that acts as a beam deflector and (b) an SEM micrograph of our metasurface structure.

$$n_t \sin \theta_t - n_i \sin \theta_i = \frac{\lambda}{2\pi} \frac{d\Phi}{dx} \qquad (1)$$

where n_t and n_i are the refractive index of the surrounding medium on the transmitted and incident sides, θ_i is the incident light angle, λ is the vacuum wavelength, and $d\Phi/dx$ is the phase gradient. In our case, $d\Phi$ equals $\pi/4$ and dx equals the unit cell size of 190 nm. Hence we expect that the gradient metasurfaces will deflect the transmitted beam at an angle of 20.48° to normal incidence.

We first performed an finite-difference time-domain (FDTD) simulation of the gradient metasurfaces. We observe that the light excites Fabry−Pérot-type resonances in each post (Figure 3a). As shown in Figure 3b, the diffraction angle observed from the phase profile is 20.48°. The same angle can also be calculated from Figure 3c by[37]

$$\theta = \sin^{-1}(k_x/k_0) = \sin^{-1}(0.35) = 20.48° \qquad (2)$$

Further, we obtain a transmission efficiency of 61% at 532 nm and an efficiency for the diffraction into the desired order of 97%. Here, these transmission and diffraction efficiencies are defined as[11,17]

$$\eta_T = I_{out}/I_{input} \qquad (3)$$

$$\eta_{diff} = I_{1rd}/I_{out} \qquad (4)$$

where I_{input} is the transmission intensity of the quartz substrate and I_{out} and I_{1rd} are the total transmission intensity and the +1 order diffraction intensity in transmission of the metasurfaces, respectively. We also define the deflection efficiency as
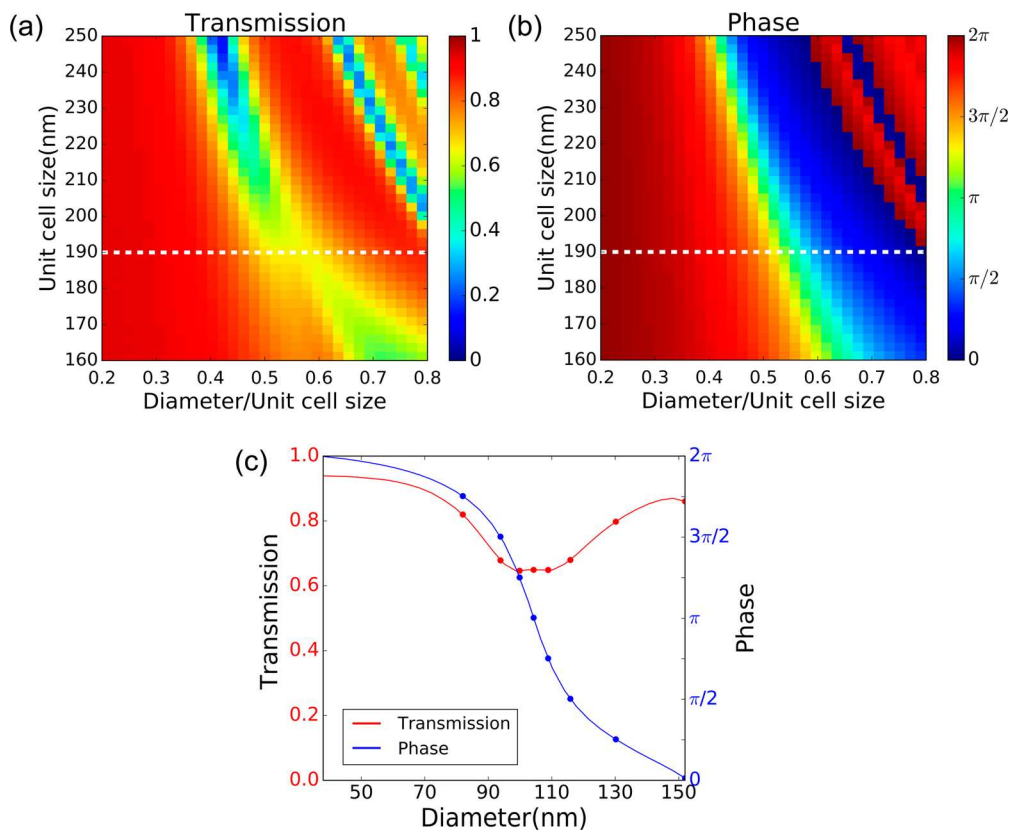
Figure 2. Calculation of (a) the transmission and (b) the phase of the periodic c-silicon posts on a square lattice with different unit cell size and diameters. (c) Transmission and phase of the periodic c-silicon posts with 190 nm unit cell size and 220 nm height for different diameters.

Table 1. Diameters of Posts with 190 nm Unit Cell Size and 220 nm Height Required to Achieve Full 2π Coverage in π/4 Steps

	phase (rad)							
	0	π/4	π/2	3π/4	π	5π/4	3π/2	7π/4
diameter (nm)	152	130	116	109	104	100	94	82

$$\eta = I_{1rd}/I_{input} \qquad (5)$$

being equal to the product of diffraction efficiency and transmission efficiency into the desired diffraction order.

The difference between unity and the observed deflection efficiencies (59%) is mainly caused by the absorption of c-silicon (30%), interface reflectivity (8%), and other diffraction orders (3%). For the 220 nm film used here, the aspect ratio of the fabricated device is 2.7. As shown in Figure 4a, we have calculated the transmission efficiency and diffraction efficiency as a function of c-silicon thickness. For thin c-silicon, it is difficult to achieve full 2π phase control for high diffraction efficiency and transmission, while for thicker c-silicon, the aspect radio is too high, leading to high absorption and fabrication complexity. It is interesting to note that if we were to use a slightly thicker film of 250 nm and a 3.4 aspect ratio, we could increase the transmission further to 73% (Figure 4b,c) even though the silicon is an absorbing material at that wavelength. Furthermore, the value is close to the result of 78% obtained with polarization-independent metasurfaces by TiO₂[31] and which requires a much higher aspect ratio and hence more demanding fabrication.

We also simulated the full-width at half-maximum (fwhm) of the diffraction efficiency for both the 220 and 250 nm metasurfaces made in c-silicon and a-silicon in Figure S3 of the Supporting Information. We obtain bandwidths around 100 and 65 nm fwhm for the c-silicon and the a-silicon metasurfaces, respectively.

Thin-film c-silicon from an SOI wafer can be transferred to a rigid or a flexible substrate using a lift-off and stamp printing process[38,39] or by adhesive wafer bonding and deep reactive ion etching (DRIE).[40,41] We used the latter method because we found it easier to maintain the integrity of the nanostructure. We then used electron beam lithography (EBL) to define the pattern. Our fabrication process is illustrated in Figure 5.

First, we deposit 1 μm silica on a SOITEC SOI wafer comprising a 220 or 250 nm thin-film c-silicon layer on 2 μm of silica. This 1 μm silica layer protects the c-silicon from the adhesives and quartz (Figure 5a). Next, we spin the UV light curable adhesive NOA61 on the sample followed by bonding to the quartz substrate (Figure 5b and c). Then the sample is illuminated by 365 nm ultraviolet LED light to cross-link the NOA61 polymer for 2 h. In order to obtain optimum adhesion, the sample is baked at 50 °C for 2 days (Figure 5d). The silicon substrate is then removed by first milling down to near 40 μm followed by DRIE (Figure 5e). Finally, the c-silicon on quartz substrate is obtained by removing the silica of the SOI wafer using HF acid.

The fabrication process of the metasurfaces on the c-silicon by EBL is shown in Figure 5g−i. The sample is spin-coated with 180 nm ZEP520A electron beam resist followed by a 50 nm aluminum layer (thermal evaporation) to serve as the charge dissipation layer. The pattern is then exposed using a

c
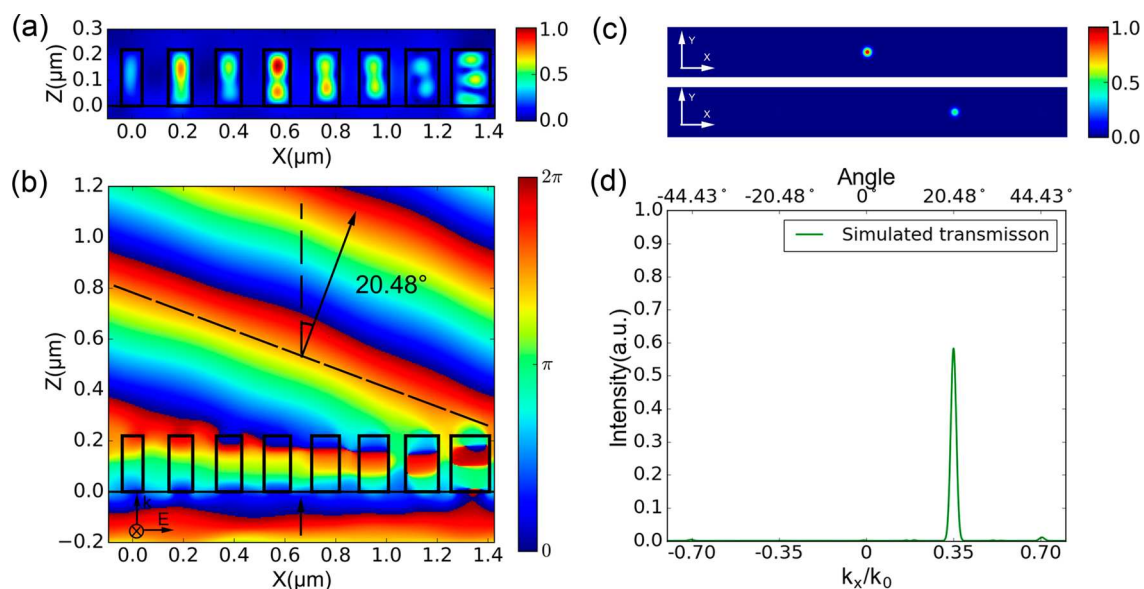
Figure 3. FDTD simulation of the gradient metasurface. (a) Mode profile for each 220 nm thick c-silicon post of the deflector, showing the magnetic field amplitude in the xz plane (H_{xz}) for a wavelength of 532 nm. We start with the smallest post on the left and gradually increase the size toward the largest post on the right. (b) Phase profile obtained by the metasurface resulting in a diffraction angle of 20.48°. (c) Far-field profiles of the incident light intensity (top) and transmission intensity (bottom). (d) Transmitted deflected beam intensity normalized to the input signal in the k_x direction.

Raith Vistec EBPG-5000plusES electron beam writer at 100 keV. After exposure, the aluminum layer is removed by tetramethylammonium hydroxide and the resist is developed with xylene. Then the pattern transfer is etched using an Oxford Instruments inductively coupled plasma tool.

The overall area of the fabricated gradient metasurface is 200 μm × 200 μm. As shown in Figure 6a, we used a 532 nm cw laser for illumination, linear polarizers, and a half-wave plate to change the polarization direction of the input light. A 4× objective (Obj1, 0.1 NA) was used to focus the light onto the sample with a spot diameter of ~150 μm. A 100× objective (Obj2, 0.9 NA) was used to collect the transmitted signal. The real-space and k-space (diffraction order) image of the sample was captured by the CCD, respectively (Figure 6a). From Figure 6b and c, we can see that the metasurface directs the light almost entirely into the +1 order, while the other diffraction orders are too weak to be captured by the CCD. The diffraction angle is measured to be 21°, which is close to the theoretical calculation and the numerical simulation. For the 220 nm thin film c-silicon design, the transmission efficiency and the diffraction efficiency are measured to be 51% and 93% by using the intensity value measured by the optical power meter. As predicted by theory, the measured transmission efficiency was polarization-independent with only 5% variation (Figure 6d). This small variation may come not only from fabrication imperfections but also from cross-talk between different meta-atoms in the array.[25] For the 250 nm thin film c-silicon design, the transmission efficiency and the diffraction efficiency can be improved to be 71% and 95% in the experiment (Figure 6e).

It is known that the transmission efficiency of plasmonic metasurfaces is limited to 25%[16] because of ohmic loss, which is absent in dielectric metasurfaces. In order to highlight the improvement achieved with different types of dielectric metasurfaces, we compare the experimental transmission in ~~the near-infrared and~~ the visible regime in Table 2. The deflection efficiency is defined as above (eq 5), being equal to

the product of diffraction efficiency and transmission efficiency. The aspect ratio is defined as the ratio of the minimum feature size of the nanostructure to the thickness of the material.

As shown in Table 2, low-index-contrast metasurfaces such as quartz[35] and TiO_2[31] offer higher transmission in the visible regime, but they also require higher thickness and very high aspect ratios to achieve a full 0 to 2π phase range for polarization-independent operation. For example, the quartz structure requires an aspect ratio of 10 for 633 nm operation, which makes it difficult to fabricate precisely. Poly-silicon and a-silicon metasurfaces can be fabricated much more easily due to their higher refractive index and lower aspect ratios. But the deflection efficiency is limited in the shorter wavelength range because of absorption loss, and reported efficiencies are below 30% at 500 nm even for polarization-dependent designs.[17] By improving the structure, Yu et al.[11] demonstrated a 45% deflection efficiency at 705 nm in a-silicon, but were not able to obtain high efficiency at 500 nm, which is very important for display applications. By comparison, c-silicon metasurfaces offer significant advantages compared to these materials. Metasurfaces based on c-Si operate with a thinner film and a lower aspect ratio than TiO_2, and they achieve better transmission than poly-silicon and a-silicon in the visible regime. On the basis of a simple transfer technique, the c-silicon can be easily transferred to the desired substrate from an SOI wafer. Due to its high refractive index, the c-silicon pattern can be easily fabricated and surrounded with other low-index materials to increase the numerical aperture of metalenses and flexible metasurfaces.[37,42]

Having now experimentally demonstrated a deflection efficiency of 47%, let us consider further improvements. First of all, we note a discrepancy of 12% between the simulated efficiency (59%, Figure 3c) and the experimental value. This discrepancy can be explained by fabrication tolerances; by analyzing the as-fabricated structures, we note an average size discrepancy in pillar diameter of 7 nm. If we use this adjusted size in our simulation, the calculated efficiency becomes 45%, i.e., similar to the experimental value within measurement error.
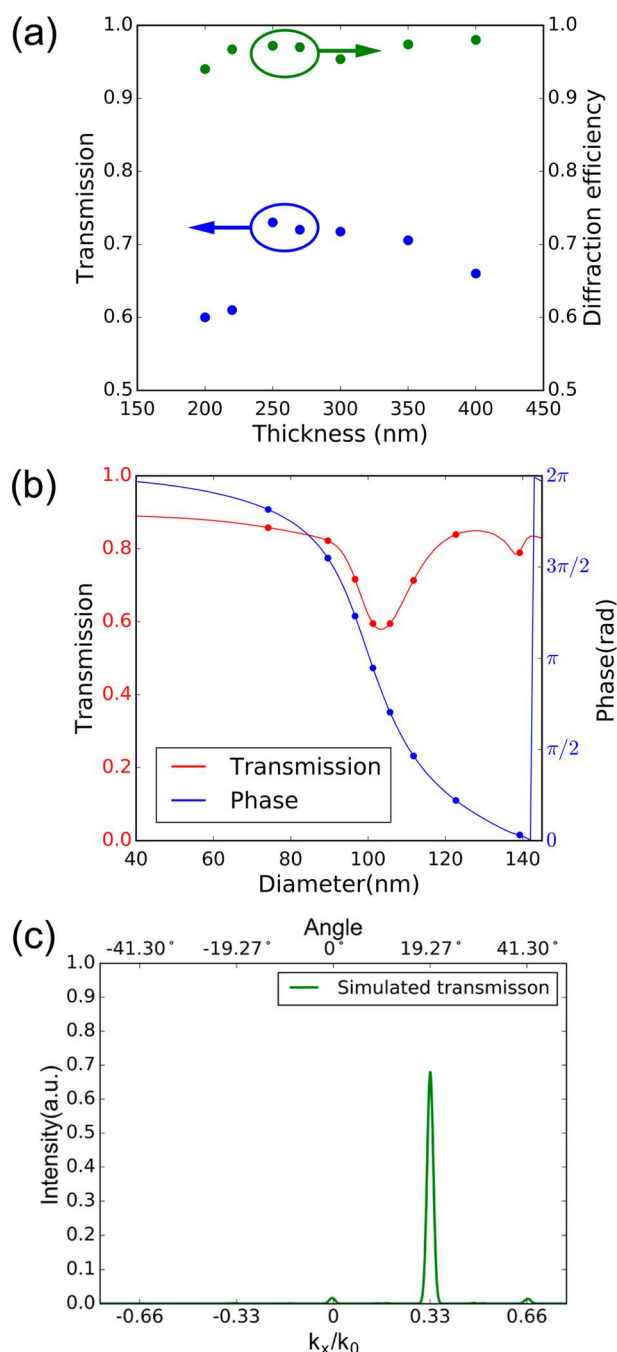
Figure 4. Calculation of (a) the transmission efficiency and diffraction efficiency of the deflectors as a function of c-silicon thickness. The corresponding meatsurface designs are shown in Table S1. (b) Transmission and phase of the periodic c-silicon posts with 200 nm unit cell size for 250 nm film thickness. (c) FDTD simulation of the transmitted beam intensity normalized to the input signal in the k_x direction for the 250 nm thick film.
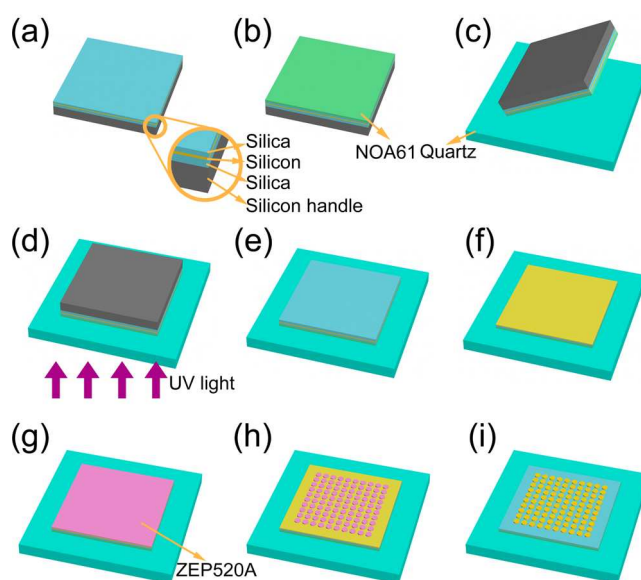

Figure 5. Schematic illustration of the c-silicon transfer process and sample fabrication. (a) Deposition of silica on an SOI wafer using ICP-CVD. (b) Spin-coating adhesive NOA61 (c) Bonding SOI with fused quartz. (d) Exposing with UV light for 2 h, followed by baking for 2 days at 50 °C. (e) Polishing the silicon substrate to ~40 μm, then removing the remaining silicon substrate by DRIE. (f) Removing the silica layer with HF acid. (g) Spinning ZEP520A and depositing Al. (h) Exposing the pattern by EBL and removing Al. (i) Transferring the pattern to silicon by ICP, then removing the resist by 1165 remover and O_2 plasma ashing.

268 It is therefore realistic to achieve the predicted 59% value with a
269 reduction in fabrication tolerances. Second, high-aspect-ratio
270 nanostructures can achieve large phase delay easily and obtain
271 high deflection efficiency. On the other hand, increased
272 thickness will also increase the absorption of the posts and
273 fabrication complexity. We found that 250 nm thickness c-
274 silicon posts happen to be the sweet spot to balance these two
275 effects and achieve the highest deflection efficiency at 532 nm.
276 Hence, we have demonstrated that an increase in film thickness

to 250 nm allows us to push the efficiency even further, i.e., up 277
to 71% in simulation (Figure 4b) and 67% in experiment 278
(Figure 6e). Demonstrating the possibility of achieving such a 279
high efficiency for visible light with silicon is a truly surprising 280
outcome of this work. We verify that diameter variations are 281
indeed responsible for the discrepancy between simulation and 282
experiment, as the variations are smaller for the 250 nm sample 283
and, correspondingly, the discrepancy is smaller as well. 284

In summary, we have transferred thin-film c-silicon onto a 285
quartz substrate by adhesive wafer bonding, then demonstrated 286
c-silicon gradient metasurfaces for beam deflection at a 287
wavelength of 532 nm. Furthermore, our experiment 288
demonstrates full 2π phase control. We demonstrate a 289
polarization-independent transmission efficiency of 71% with 290
95% diffraction efficiency. The corresponding deflection 291
efficiency is 67%, and our simulations show that it can be 292
increased up to 71%, which is very close to the values achieved 293
with TiO_2, yet with a lower aspect ratio, hence reduced 294
fabrication complexity, if we use commercially available silicon 295
on glass samples.[44,45] This lower aspect ratio also achieved high 296
phase delay while reducing the absorption and fabrication 297
complexity, which make it possible to achieve high efficiency 298
metasurfaces comparable with TiO_2. 299

We believe that this approach not only can be applied to 300
other wavefront shaping situations, such as focusing, vortex 301
generation, and holography, but also offers a viable route to 302
efficient tunable metasurfaces on flexible substrates in the 303
visible range. Our geometry is also attractive for a variety of 304
applications in integrated optics, such as imaging, biomedical 305
sciences, or wearable consumer electronics. 306
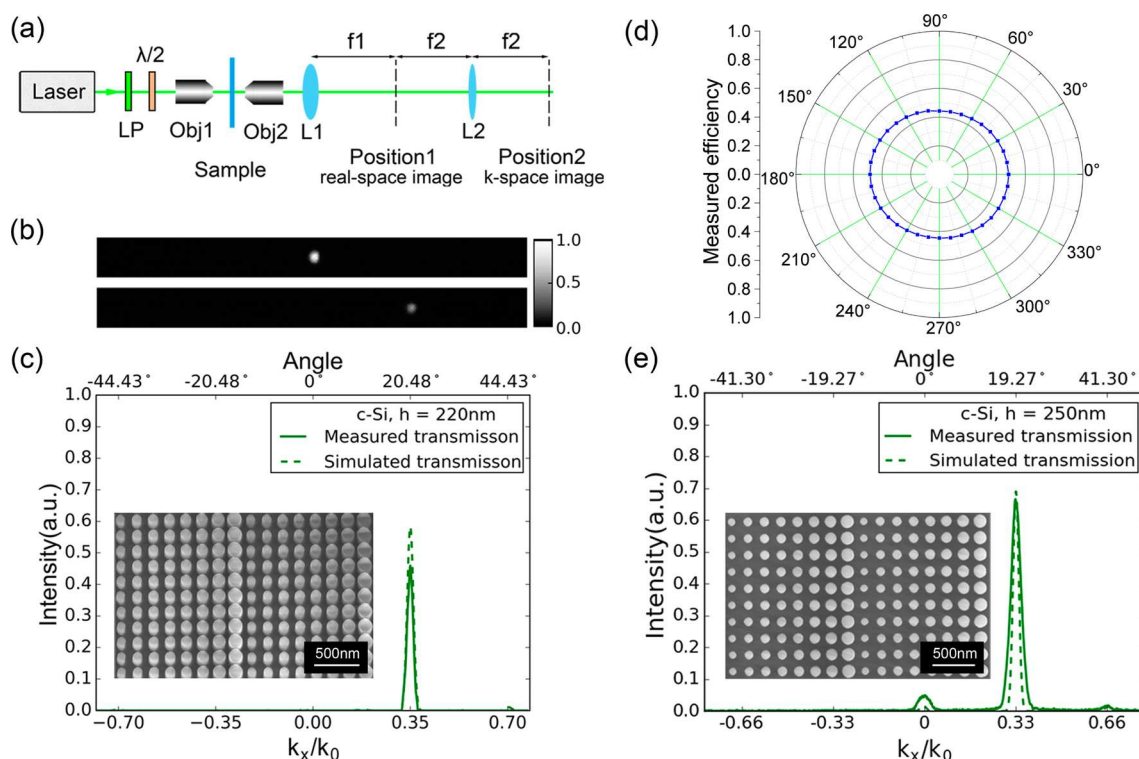
Figure 6. (a) Measurement setup used to characterize the metasurfaces according to the design shown in Table 1. (b) Far-field profiles of the incident light intensity (top) and transmitted intensity (bottom) captured by a CCD camera. (c) Experiment (solid line, calculated from the CCD camera data in panel b) and simulation (dashed line, same as Figure 3c) of the transmitted deflected beam intensity normalized to the input signal in the k_x direction of the 220 nm thin film c-silicon design. The inset shows an SEM micrograph of the structure. (d) Measured transmission efficiency with different polarization directions of the 220 nm thin film c-silicon design. The polarization direction is defined as the angle between the electric field and gradient of the posts. (e) Experiment and simulation of the transmitted deflected beam intensity of the 250 nm thin film c-silicon design.

Table 2. Summary of Previously Reported Experimental Metasurfaces Used as Deflectors Operating in Transmission in the Visible Range

ref	material	wavelength	deflection efficiency	polarization	building block	thickness	aspect ratio
Chen et al.[35]	quartz	633 nm	55%	independence	square posts	1.38 μm	10
Astilean et al.[43]	TiO$_2$	633 nm	85%	linear	1D grating	540 nm	5.3
Lalanne et al.[31]	TiO$_2$	633 nm	78%	independence	square posts	487 nm	4.6
Yu et al.[11]	a-silicon	705 nm	45%	independence	circular posts	130 nm	0.93
Lin et al.[17]	p-silicon	500 nm	29%	circular	nanobeams	100 nm	1.2
this work (experiment)	c-silicon	532 nm	47%	independence	circular posts	220 nm	2.47
this work (simulation)	c-silicon	532 nm	59%	independence	circular posts	220 nm	2.7
this work (experiment)	c-silicon	532 nm	67%	independence	circular posts	250 nm	3.4
this work (simulation)	c-silicon	532 nm	71%	independence	circular posts	250 nm	3.4

■ ASSOCIATED CONTENT

Ⓢ Supporting Information

The Supporting Information is available free of charge on the ACS Publications website at DOI: 10.1021/acsphotonics.6b00740.

Simulation of the deflecting achieved by our metasurfaces for c-silicon and a-silicon; the parameter and bandwidth of our designed metasurfaces. (PDF)

■ AUTHOR INFORMATION

Corresponding Author

*E-mail: wangxueh@mail.sysu.edu.cn.

ORCID Ⓘ

Zhenpeng Zhou: 0000-0001-9712-0866

Author Contributions

‖Z. Zhou and J. Li contributed equally to this work.

Notes

The authors declare no competing financial interest.

also would like to acknowledge Prof. Jianwen Dong for useful discussions on the metasurface design.

■ REFERENCES

(1) Zheludev, N. I.; Kivshar, Y. S. From metamaterials to metadevices. *Nat. Mater.* **2012**, *11*, 917−924.

(2) Meinzer, N.; Barnes, W. L.; Hooper, I. R. Plasmonic meta-atoms and metasurfaces. *Nat. Photonics* **2014**, *8*, 889−898.

(3) Yu, N.; Capasso, F. Flat optics with designer metasurfaces. *Nat. Mater.* **2014**, *13*, 139−150.

(4) Minovich, A. E.; Miroshnichenko, A. E.; Bykov, A. Y.; Murzina, T. V.; Neshev, D. N.; Kivshar, Y. S. Functional and nonlinear optical metasurfaces. *Laser Photonics Rev.* **2015**, *9*, 195−213.

(5) Glybovski, S. B.; Tretyakov, S. A.; Belov, P. A.; Kivshar, Y. S.; Simovski, C. R. Metasurfaces: From microwaves to visible. *Phys. Rep.* **2016**, *634*, 1−72.

(6) Wan, C.; Ho, Y.; Nunez-Sanchez, S.; Chen, L.; Lopez-Garcia, M.; Pugh, J.; Zhu, B.; Selvaraj, P.; Mallick, T.; Senthilarasu, S.; Cryan, M. J. A selective metasurface absorber with an amorphous carbon interlayer for solar thermal applications. *Nano Energy* **2016**, *26*, 392−397.

(7) West, P. R.; Ishii, S.; Naik, G. V.; Emani, N. K.; Shalaev, V. M.; Boltasseva, A. Searching for better plasmonic materials. *Laser Photonics Rev.* **2010**, *4*, 795−808.

(8) Yu, N.; Genevet, P.; Kats, M. A.; Aieta, F.; Tetienne, J. P.; Capasso, F.; Gaburro, Z. Light propagation with phase discontinuities: generalized laws of reflection and refraction. *Science* **2011**, *334*, 333−337.

(9) Fattal, D.; Li, J.; Peng, Z.; Fiorentino, M.; Beausoleil, R. G. Flat dielectric grating reflectors with focusing abilities. *Nat. Photonics* **2010**, *4*, 466−470.

(10) Jahani, S.; Jacob, Z. All-dielectric metamaterials. *Nat. Nanotechnol.* **2016**, *11*, 23−36.

(11) Yu, Y. F.; Zhu, A. Y.; Paniagua-Domínguez, R.; Fu, Y. H.; Luk'yanchuk, B.; Kuznetsov, A. I. High-transmission dielectric metasurface with 2π phase control at visible wavelengths. *Laser Photonics Rev.* **2015**, *9*, 412−418.

(12) Moitra, P.; Slovick, B. A.; Gang, Y. Z.; Krishnamurthy, S.; Valentine, J. Experimental demonstration of a broadband all-dielectric metamaterial perfect reflector. *Appl. Phys. Lett.* **2014**, *104*, 171102.

(13) Esfandyarpour, M.; Garnett, E. C.; Cui, Y.; McGehee, M. D.; Brongersma, M. L. Metamaterial mirrors in optoelectronic devices. *Nat. Nanotechnol.* **2014**, *9*, 542−547.

(14) Staude, I.; Miroshnichenko, A. E.; Decker, M.; Fofang, N. T.; Liu, S.; Gonzales, E.; Dominguez, J.; Luk, T. S.; Neshev, D. N.; Brener, I.; Kivshar, Y. Tailoring directional scattering through magnetic and electric resonances in subwavelength silicon nanodisks. *ACS Nano* **2013**, *7*, 7824−7832.

(15) Decker, M.; Staude, I.; Falkner, M.; Dominguez, J.; Neshev, D. N.; Brener, I.; Pertsch, T.; Kivshar, Y. S. High-Efficiency Dielectric Huygens' Surfaces. *Adv. Opt. Mater.* **2015**, *3*, 813−820.

(16) Arbabi, A.; Horie, Y.; Ball, A. J.; Bagheri, M.; Faraon, A. Subwavelength-thick lenses with high numerical apertures and large efficiency based on high-contrast transmitarrays. *Nat. Commun.* **2015**, *6*, 7069.

(17) Lin, D.; Fan, P.; Hasman, E.; Brongersma, M. L. Dielectric gradient metasurface optical elements. *Science* **2014**, *345*, 298−302.

(18) Klemm, A. B.; Stellinga, D.; Martins, E. R.; Lewis, L.; Huyet, G.; O'Faolain, L.; Krauss, T. F. Experimental high numerical aperture focusing with high contrast gratings. *Opt. Lett.* **2013**, *38*, 3410−3413.

(19) Aieta, F.; Kats, M. A.; Genevet, P.; Capasso, F. Applied optics. Multiwavelength achromatic metasurfaces by dispersive phase compensation. *Science* **2015**, *347*, 1342−1345.

(20) Chong, K. E.; Staude, I.; James, A.; Dominguez, J.; Liu, S.; Campione, S.; Subramania, G. S.; Luk, T. S.; Decker, M.; Neshev, D. N.; Brener, I.; Kivshar, Y. S. Polarization-Independent Silicon Metadevices for Efficient Optical Wavefront Control. *Nano Lett.* **2015**, *15*, 5369−5374.

(21) Shalaev, M. I.; Sun, J.; Tsukernik, A.; Pandey, A.; Nikolskiy, K.; Litchinitser, N. M. High-Efficiency All-Dielectric Metasurfaces for Ultracompact Beam Manipulation in Transmission Mode. *Nano Lett.* **2015**, *15*, 6261−6266.

(22) Khorasaninejad, M.; Ambrosio, A.; Kanhaiya, P.; Capasso, F. Broadband and chiral binary dielectric meta-holograms. *Sci. Adv.* **2016**, *2*, e1501258.

(23) Wang, B.; Dong, F.; Li, Q. T.; Yang, D.; Sun, C.; Chen, J.; Song, Z.; Xu, L.; Chu, W.; Xiao, Y. F.; Gong, Q.; Li, Y. Visible-Frequency Dielectric Metasurfaces for Multiwavelength Achromatic and Highly Dispersive Holograms. *Nano Lett.* **2016**, *16*, 5235−5240.

(24) Chong, K. E.; Wang, L.; Staude, I.; James, A. R.; Dominguez, J.; Liu, S.; Subramania, G. S.; Decker, M.; Neshev, D. N.; Brener, I.; Kivshar, Y. S. Efficient Polarization-Insensitive Complex Wavefront Control Using Huygens' Metasurfaces Based on Dielectric Resonant Meta-atoms. *ACS Photonics* **2016**, *3*, 514−519.

(25) Li, Q.-T.; Dong, F.; Wang, B.; Gan, F.; Chen, J.; Song, Z.; Xu, L.; Chu, W.; Xiao, Y.-F.; Gong, Q.; Li, Y. Polarization-independent and high-efficiency dielectric metasurfaces for visible light. *Opt. Express* **2016**, *24*, 16309.

(26) Yang, Y.; Wang, W.; Boulesbaa, A.; Kravchenko, II; Briggs, D. P.; Puretzky, A.; Geohegan, D.; Valentine, J. Nonlinear Fano-Resonant Dielectric Metasurfaces. *Nano Lett.* **2015**, *15*, 7388−7393.

(27) Arbabi, A.; Horie, Y.; Bagheri, M.; Faraon, A. Dielectric metasurfaces for complete control of phase and polarization with subwavelength spatial resolution and high transmission. *Nat. Nanotechnol.* **2015**, *10*, 937−943.

(28) Backlund, M. P.; Arbabi, A.; Petrov, P. N.; Arbabi, E.; Saurabh, S.; Faraon, A.; Moerner, W. E. Removing Orientation-Induced Localization Biases in Single-Molecule Microscopy Using a Broadband Metasurface Mask. *Nat. Photonics* **2016**, *10*, 459−462.

(29) Palik, E. D. *Handbook of Optical Constants of Solids*; Academic Press: San Diego, 1985.

(30) Evlyukhin, A. B.; Novikov, S. M.; Zywietz, U.; Eriksen, R. L.; Reinhardt, C.; Bozhevolnyi, S. I.; Chichkov, B. N. Demonstration of magnetic dipole resonances of dielectric nanospheres in the visible region. *Nano Lett.* **2012**, *12*, 3749−3755.

(31) Lalanne, P.; Astilean, S.; Chavel, P.; Cambril, E.; Launois, H. Blazed binary subwavelength gratings with efficiencies larger than those of conventional échelette gratings. *Opt. Lett.* **1998**, *23*, 1081.

(32) Khorasaninejad, M.; Chen, W. T.; Devlin, R. C.; Oh, J.; Zhu, A. Y.; Capasso, F. Metalenses at visible wavelengths: Diffraction-limited focusing and subwavelength resolution imaging. *Science* **2016**, *352*, 1190−1194.

(33) Khorasaninejad, M.; Zhu, A. Y.; Roques-Carmes, C.; Chen, W. T.; Oh, J.; Mishra, I.; Devlin, R. C.; Capasso, F. Polarization-Insensitive Metalenses at Visible Wavelengths. *Nano Lett.* **2016**, *16*, 7229−7234.

(34) Zhan, A.; Colburn, S.; Trivedi, R.; Fryett, T. K.; Dodson, C. M.; Majumdar, A. Low-Contrast Dielectric Metasurface Optics. *ACS Photonics* **2016**, *3*, 209−214.

(35) Chen, F. T.; Craighead, H. G. Diffractive phase elements based on two-dimensional artificial dielectrics. *Opt. Lett.* **1995**, *20*, 121−123.

(36) Li, L. New formulation of the Fourier modal method for crossed surface-relief gratings. *J. Opt. Soc. Am. A* **1997**, *14*, 2758.

(37) Ee, H. S.; Agarwal, R. Tunable Metasurface and Flat Optical Zoom Lens on a Stretchable Substrate. *Nano Lett.* **2016**, *16*, 2818−2823.

(38) Meitl, M. A.; Zhu, Z.-T.; Kumar, V.; Lee, K. J.; Feng, X.; Huang, Y. Y.; Adesida, I.; Nuzzo, R. G.; Rogers, J. A. Transfer printing by kinetic control of adhesion to an elastomeric stamp. *Nat. Mater.* **2006**, *5*, 33−38.

(39) Xu, X.; Subbaraman, H.; Hosseini, A.; Lin, C. Y.; Kwong, D.; Chen, R. T. Stamp printing of silicon-nanomembrane-based photonic devices onto flexible substrates with a suspended configuration. *Opt. Lett.* **2012**, *37*, 1020−1022.

(40) Niklaus, F.; Stemme, G.; Lu, J. Q.; Gutmann, R. J. Adhesive wafer bonding. *J. Appl. Phys.* **2006**, *99*, 031101.

(41) Zablocki, M. J.; Sharkawy, A.; Ebil, O.; Prather, D. W. Nanomembrane transfer process for intricate photonic device applications. *Opt. Lett.* **2011**, *36*, 58−60.

472 (42) Zhu, L.; Kapraun, J.; Ferrara, J.; Chang-Hasnain, C. J. Flexible
473 photonic metastructures for tunable coloration. *Optica* **2015**, *2*, 255.
474 (43) Astilean, S.; Lalanne, P.; Chavel, P.; Cambril, E.; Launois, H.
475 High-efficiency subwavelength diffractive element patterned in a high-
476 refractive-index material for 633 nm. *Opt. Lett.* **1998**, *23*, 552−554.
477 (44) Kim, H. S.; Blick, R. H.; Kim, D. M.; Eom, C. B. Bonding
478 silicon-on-insulator to glass wafers for integrated bio-electronic
479 circuits. *Appl. Phys. Lett.* **2004**, *85*, 2370−2372.
480 (45) MEMS Engineering and Material Home Page. http://www.
481 memsengineering.com (accessed January 30, 2017).